ACS OMEGA

http://pubs.acs.org/journal/acsodf

Article

$CsPbBr_3$ Perovskite Nanocrystals for a Q-Switched Pulsed Fiber Laser in the C-Band Region

Shaohong Guo, Chunxia Li, Heng Jia,* and Nan Li*

Cite This: *ACS Omega* 2022, 7, 45504−45509

Read Online

ACCESS | Metrics & More | Article Recommendations

ABSTRACT: All-inorganic perovskite nanocrystals have been widely reported as promising light-harvesting and light-emitting semiconductor nanomaterials. However, their nonlinear optical properties and laser applications have rarely been explored, especially for pulse laser modulation in the telecommunication C-band window. Herein, we experimentally demonstrated a passively Q-switched erbium-doped fiber laser (EDFL) operation at the C-band region using perovskite $CsPbBr_3$ nanocrystals as a saturable absorber (SA). The broadband linear optical absorption in the 300−2000 nm range and the nonlinear optical absorption at the C-band range of around 1560 nm were discovered and investigated in $CsPbBr_3$ nanocrystals. The $CsPbBr_3$-based SA exhibited good saturable absorption performance with a modulation depth and saturation intensity equivalent to 19.1% and 10.9 MW/cm^2, respectively. By integrating the $CsPbBr_3$ SA into an EDFL cavity, a passively Q-switched operation with a central wavelength of 1560 nm, a threshold pump power of 60 mW, and the shortest pulse duration of 5.96 μs was achieved. In addition, such a Q-switching operation exhibited long-term stability. Our results indicate that the $CsPbBr_3$ perovskite nanocrystals can serve as an efficient candidate for constructing pulsed lasers in the C-band or even longer NIR wavelength region.

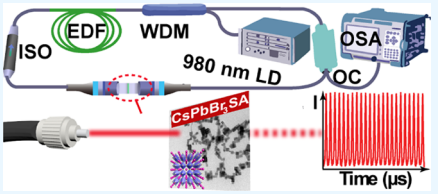

1. INTRODUCTION

Pulsed lasers are promising tools in many fields of scientific research and industry because of their favorable properties of large pulse energy and high peak power, including biomedicine, spectroscopy, optical communications, laser processing, and others.[1−5] In general, the passive Q-switching technique is one of the most practical for generating pulsed lasers due to its many advantages.[6,7] In such passive Q-switching lasers, saturable absorbers (SAs) are employed as nonlinear optical modulators, whose transmittance increases as the input laser intensity increases, thus allowing continuous wave lasers into pulsed lasers. Over the past decades, numerous efforts have been dedicated to developing SA materials including graphene,[8,9] carbon nanotubes (CNTs),[6,10] topological insulators (TIs),[11,12] transition-metal dichalcogenides (TMDs),[13,14] transition-metal oxides (TMOs),[15−19] black phosphorus (BP),[20] and semiconducting polymer dots (Pdots).[21,22] However, these SAs suffer from their inherent limitations. For example, graphene suffers from relatively low modulation depth, while CNTs require precise control of their diameter for generating a specific absorption spectrum.[23] TIs need complicated preparation processes.[24] TMDs and TMOs generally have large band gaps.[25] Furthermore, BP is easily oxidized,[26] and Pdots require complex tuning in broadband operation.[22] Therefore, it is of great significance to explore new SA materials for realizing potential applications in a Q-switched pulsed laser.

$CsPbBr_3$ perovskite nanocrystals (PNCs), as one of the most efficient optical materials, have recently drawn considerable attention due to their attractive properties, such as large absorption coefficient, low defect density, high gain value, high charge-carrier mobility, and low saturation intensity.[27,28] These properties make them promising candidates for optoelectronic devices, especially in laser applications.[29,30] In the last few years, significant efforts have been devoted to synthesizing $CsPbBr_3$ PNCs, investigating their nonlinear optical absorption performances, and exploiting their potential in the field of pulse laser engineering.[31,32] For instance, as early as 2016, Zhou et al. used $CsPbBr_3$ nanocrystals as SAs for generating mode-locking pulses in the ∼1 μm wavelength region.[33] Subsequently, in 2017, Li et al. reported the Q-switched pulses generation in the visible wavelength range (515 nm) using $CsPbBr_3$ perovskite quantum dots as SAs.[34] Recently, Liu et al. and Zhou et al. have demonstrated that $CsPbBr_3$ nanocrystals have the potential to realize pulsed laser modulation by mode locking at ∼1.6 and ∼2 μm regions, respectively.[35,36] To the best of our knowledge, despite the significant research efforts described above, pulsed laser generation with $CsPbBr_3$ nanocrystals in the telecommunication window of the C-band has not been reported to date. The C-band (1530−1565

Received: September 21, 2022
Accepted: November 14, 2022
Published: November 28, 2022

https://doi.org/10.1021/acsomega.2c06107
ACS Omega 2022, 7, 45504−45509

nm) has been regarded as one of the most promising regimes for optical communication applications due to its lower fiber loss and lower optical nonlinearity in fiber optic communication systems.[37,38] Thus, exploring the nonlinear optical properties and related laser applications of the perovskite nanomaterials at the C-band region has great significance.

In this work, we demonstrated the pulsed laser generation operating at the C-band telecommunication wavelength based on the $CsPbBr_3$ SA (Scheme 1). The $CsPbBr_3$ PNCs with an average particle size of ∼20 nm were synthesized by a hot injection method, and linear and nonlinear optical properties of the PNCs in the near-infrared region were systematically investigated. By inserting $CsPbBr_3$ PNC-based SA between two fiber connectors in an erbium-doped fiber laser (EDFL), stable Q-switched pulses generating in the C-band region with a central wavelength of 1560 nm were successfully achieved. Our results showed that the $CsPbBr_3$ PNCs can be promising SA candidates for the generation of Q-switched laser pulses in the C-band and hold great potential to extend the region of nonlinear responses for broadband optical applications.

Scheme 1. Schematic Diagram of Passively Q-Switched Operation for Pulsed Laser Generation at the C-Band Region Based on $CsPbBr_3$ PNCs SA

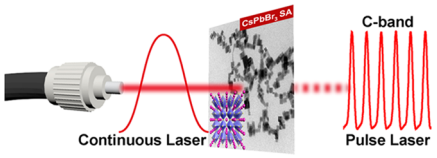

2. RESULTS AND DISCUSSION

2.1. Fabrication and Characterizations of $CsPbBr_3$ PNCs. In our experiment, the manufacturing process requires two steps to obtain $CsPbBr_3$ PNC-based SA film. First, the $CsPbBr_3$ nanocrystals were synthesized by the hot injection method according to the previously reported literature with a similar procedure.[39] Briefly, $PbBr_2$ (0.18 mmol) was added into a 50 mL two-necked flask containing a mixture of oleic acid (OA, 0.8 mL), oleylamine (OAm, 0.8 mL), and 1-octadecene (ODE, 5 mL). The resulting solution was evacuated and refilled with nitrogen for 30 min at 120 °C. After that, the solution was heated to 185 °C and OAm (0.8 mL) and OA (0.8 mL) were injected. Subsequently, the Cs-oleate (64 μL) was quickly injected into the solution and the mixture was cooled in an ice bath for 5 s. The as-obtained $CsPbBr_3$ PNCs were collected by centrifugation, washed with hexane and ethyl acetate, and finally redispersed in acetone and toluene (1:3). In the second step, the as-prepared $CsPbBr_3$ PNC liquid solution and 15 wt % acetone solution of polymethylmethacrylate (PMMA) were mixed (volume ratio 1:1) by ultrasonication. Then, the mixed solution was kept for 24 h and without any precipitates. The $CsPbBr_3$-based SA film was prepared by dropping the solution onto a glass substrate, followed by drying at room temperature.

The morphology, size, and nanostructure of the prepared $CsPbBr_3$ sample were studied by transmission electron microscopy (TEM), high-resolution TEM (HRTEM) combined with selected area electron diffraction (SAED), and X-ray diffraction (XRD). TEM image shows that the as-prepared $CsPbBr_3$ nanoparticles are nearly cubic in shape with a size of around 20 nm (Figure 1a,b). The HRTEM image and the corresponding SAED pattern indicate the single-crystalline nature of the $CsPbBr_3$ nanocrystals, as shown in Figure 1c,d. The clear lattice fringes were determined to be 0.59 nm, which corresponds to the d spacing for the (001) crystal plane of the monoclinic $CsPbBr_3$ perovskite structure. The structure schematic of $CsPbBr_3$ PNCs is represented in Figure 1e, in which the inorganic cage of $PbBr_6$ octahedra shares corners to form a three-dimensional network, and the larger Cs-site cations are localized in the 12-coordinate cubo-octahedral cavities within the network.[34] X-ray diffraction (XRD) is further characterized to confirm the crystal structure of the obtained $CsPbBr_3$ perovskite samples. As shown in Figure 1f, the main diffraction peaks at 2θ values of 15.1, 21.5, 30.6, 34.4, 37.8, and 43.7° are assigned to the (100), (110), (200), (201), (211), and (202) planes of the reported monoclinic phase of $CsPbBr_3$ (JCPDS No. 18-0364), demonstrating the formation of pure monoclinic $CsPbBr_3$ structure.[40]

To further determine the chemical composition and elemental distribution of the resulting $CsPbBr_3$ PNCs, energy-dispersive X-ray spectroscopy (EDX) measurement was performed. As shown in Figure 2a, the EDX spectrum confirms the existence of Cs, Pb, and Br elements in the PNCs, except for most of the signals of C and Cu from the carbon-

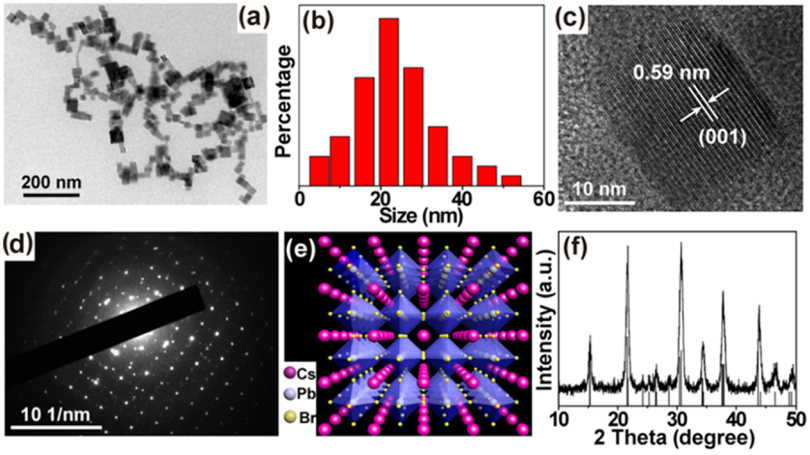

Figure 1. (a) TEM image of $CsPbBr_3$ PNCs. (b) Size distribution histogram of $CsPbBr_3$ PNCs. (c) HRTEM image of a single $CsPbBr_3$ PNC. (d) SAED pattern of $CsPbBr_3$ PNCs. (e) Structure schematic of $CsPbBr_3$ perovskite lattice. (f) XRD profile of $CsPbBr_3$ PNCs.

https://doi.org/10.1021/acsomega.2c06107
ACS Omega 2022, 7, 45504−45509

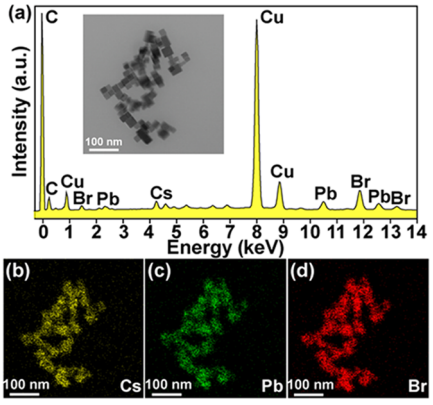

Figure 2. EDX spectrum (a) and STEM image (inset) of $CsPbBr_3$ PNCs, and its corresponding element mapping images of (b) Cs, (c) Pb, and (d) Br.

supported copper grid. Furthermore, the corresponding element mapping images obtained by scanning randomly chosen PNCs (inset of Figure 2a) reveal the uniform distribution of Cs, Pb, and Br elements in the whole region of the cubic nanoparticles (Figure 2b–d), further indicating the successful synthesis of $CsPbBr_3$ PNCs.

2.2. Linear and Nonlinear Optical Properties of $CsPbBr_3$ PNCs-Based SA. To better investigate the linear optical property of the $CsPbBr_3$ PNCs, we first measured and compared the optical absorption in the wavelength range of 300–2000 nm of the $CsPbBr_3$ PNCs colloidal solution and the $CsPbBr_3$ PNCs film. As represented in Figure 3a, the $CsPbBr_3$ solution displays a strong band gap absorption ranging from 300 to 600 nm and a broad and relatively weak optical absorption from 600 to 2000 nm. As a comparison, the absorption spectrum of $CsPbBr_3$ film with the same concentration was also measured. As shown in Figure 3b, a remarkably enhanced absorption in the NIR spectral region (800–2000 nm) can be observed in the $CsPbBr_3$ film. While the film without $CsPbBr_3$ PNCs shows a very weak absorption in the entire range from 300 to 2000 nm. The significantly enhanced absorption of $CsPbBr_3$ film in the NIR region may be caused by edge states and crystallographic defects of the PNCs film,[33,35,36] which endow the $CsPbBr_3$ nanomaterials with the potential to serve as SAs for pulsed laser generation in the NIR wavelength range.

Subsequently, saturable absorption characteristics of the $CsPbBr_3$ PNCs film were also investigated. The relationship between the transmission ratio of the film and the corresponding pump power density was measured using a homemade pulsed fiber laser at 1560 nm with a repetition rate of 34 MHz and a pulse width of 800 fs. Figure 3c shows the obtained data fitted by the formula $\alpha(I) = \alpha_s/(1 + I/I_s) + \alpha_{ns}$ (where $\alpha(I)$ is the absorption coefficient, α_s and α_{ns} are the saturable and nonsaturable absorption components, respectively, and I and I_s are the input and saturable intensities, respectively).[41,42] Using the formula, the corresponding values of modulation depth, saturation intensity, and nonsaturable loss were calculated to be 19.1%, 10.9 MW/cm^2, and 31.2%, respectively. These results indicated that the $CsPbBr_3$ PNCs film possessed the potential for constructing pulsed lasers in the C-band region.

2.3. Q-Switched Pulsed Laser Generation in the C-band Region. To evaluate the feasibility of $CsPbBr_3$ PNCs as a SA for laser application, a Q-switched fiber laser system was constructed, as shown in Figure 4. The system consists of a pump source, a 980/1550 nm wavelength division multiplexer (WDM), an erbium-doped fiber (EDF), a polarization-

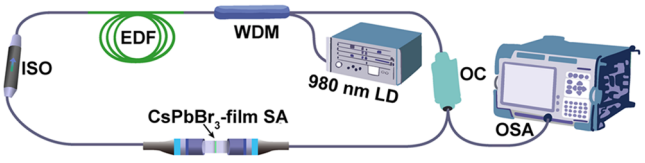

Figure 4. Schematic illustration of the self-built erbium-doped fiber laser (EDFL) system with a $CsPbBr_3$-based SA.

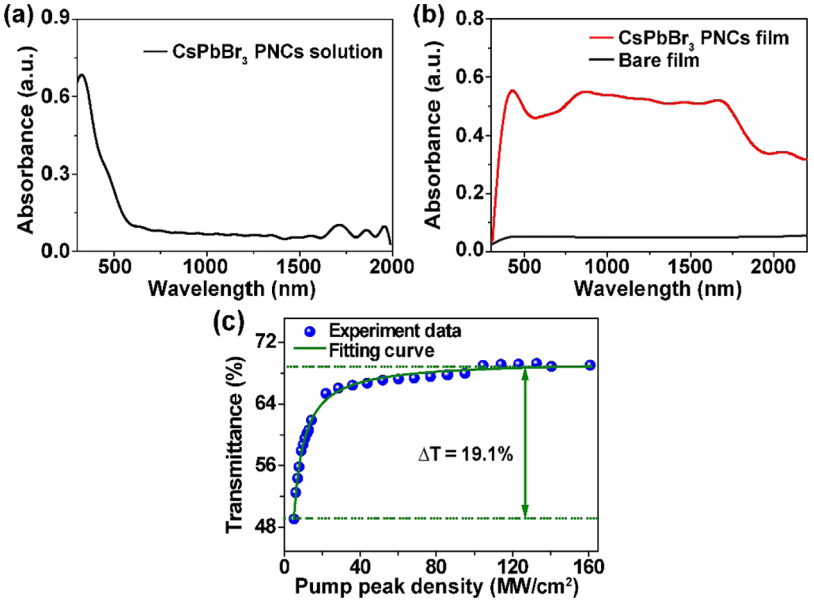

Figure 3. (a) Absorption spectrum of the $CsPbBr_3$ PNCs solution. (b) Absorption spectra of the film with and without $CsPbBr_3$ PNCs. (c) Relationship between the transmittance of the $CsPbBr_3$ PNCs film at 1560 nm and the pump peak density.

https://doi.org/10.1021/acsomega.2c06107
ACS Omega 2022, 7, 45504–45509

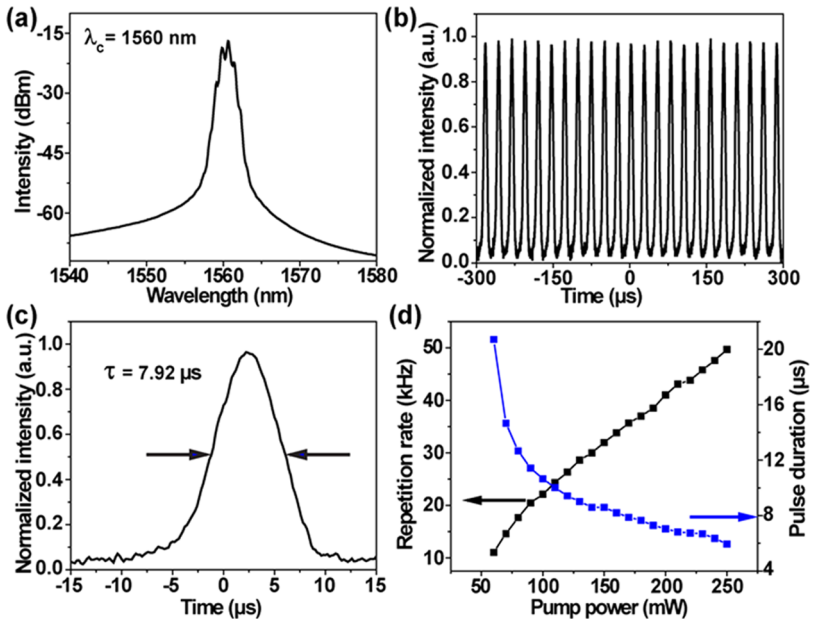

Figure 5. Q-switched pulse output results in the EDFL cavity based on $CsPbBr_3$ PNCs SA. (a) Q-switching optical spectrum at C-band. (b) Typical Q-switching pulse train. (c) Single Q-switching pulse profile. (d) Pulse duration and repetition rate as functions of pump power, respectively.

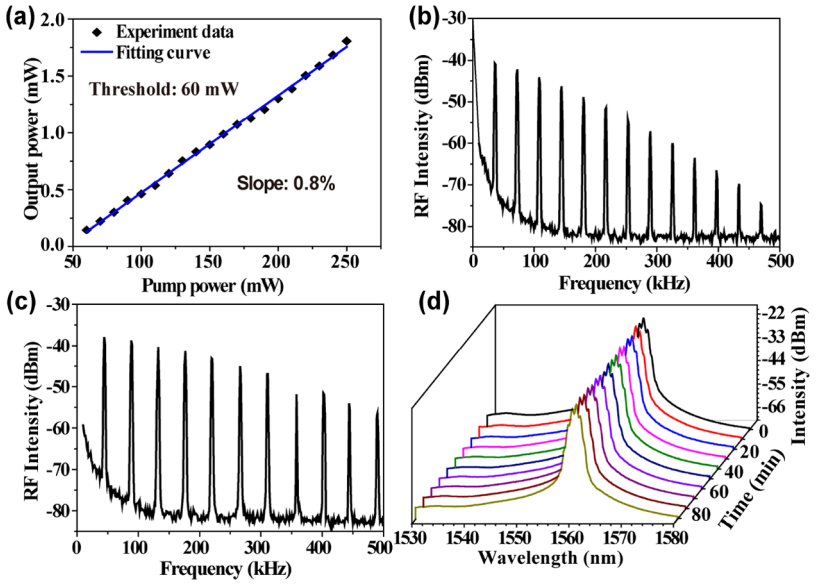

Figure 6. (a) Output power of the Q-switched EDFL as a function of the pump power. Radio-frequency spectra of the Q-switched fiber laser operating at 35.7 kHz (b) and 43.8 kHz (c). (d) Time-dependent emission spectra of the Q-switched laser at C-band recorded at 10 min intervals.

independent isolator (PI-ISO), an optical coupler (OC), and a $CsPbBr_3$ PNC film-based SA. Specifically, a 980 nm laser diode (LD) was used as the pump source, which could reach the maximum output power of 800 mW. The 980/1550 nm WDM was employed to couple the pump light into a laser cavity. Also, a 23 cm long EDF was used as the gain medium, which was pumped via the 980/1550 nm WDM. The EDF has core/cladding dimensions of 8/125 μm, a numerical aperture of 0.2, and an absorption of 80 dB/m at 1530 nm. The total EDFL cavity length is about 5.4 m. In addition, the PI-ISO was used to guarantee the unidirectional transmission of the laser operation. The $CsPbBr_3$ SA was sandwiched between two fiber connectors of the EDFL cavity to induce Q-switched operation. The generated pulse laser signals were exported through the 10 dB OC and analyzed using an optical spectrum analyzer, a digital oscilloscope with a 12.5 GHz photodetector, and a power meter.

Next, the laser output performance was systematically investigated. Figure 5 exhibits the Q-switched results with the $CsPbBr_3$ SA. The fiber laser started to operate in a continuous wave regime at a pump power near 60 mW. By gradually increasing the pump power from 60 to 250 mW, the Q-switching operation state can be clearly observed. The emission spectrum of the Q-switched EDFL at a pump power of ~190 mW is shown in Figure 5a. The emission wavelength centers at ~1560 nm, showing that the typical Q-switched laser output in the C-band of optical telecommunications was obtained. Figure 5b exhibits the corresponding pulse train of

https://doi.org/10.1021/acsomega.2c06107
ACS Omega 2022, 7, 45504−45509

the Q-switching operation. The interval time between two adjacent pulses is determined to be 25.87 μs with a repetition rate of 38.7 kHz. The single pulse profile is represented in Figure 5c. A pulse duration of 7.92 μs was obtained. Figure 5d shows the dependences of pulse duration and repetition rate on pump power. As the pump power was increased from 60 to 250 mW, the pulse duration varied from 20.73 to 5.96 μs, and the corresponding repetition rate could be changed between 10.97 and 49.70 kHz. It was clearly observed that the pulse duration decreased and the repetition rate increased with the increase of the pump power, which indicated a typical passively Q-switched laser feature.

Furthermore, we further investigated the output power of the Q-switched laser as a function of the pump power. As shown in Figure 6a, the output power exhibited a linear increase with the increase of pump power from 60 to 250 mW, and the maximum output power was about 1.9 mW, corresponding to a slope efficiency of ∼0.8%. The radio-frequency spectra of the Q-switching operation in different regimes are given in Figure 6b,c. The signal-to-noise ratio (SNR) of the frequency peaks at ∼35.7 and 43.8 kHz were measured to be ∼34 and 37 dB, respectively, indicating a good Q-switching operation. In addition, it should be pointed out that the long-term stability of laser operation is of great significance for wide and potential applications. To examine the stability of the Q-switched laser operation based on $CsPbBr_3$ SA, we monitored the output spectra every 10 min for 1.5 h, as represented in Figure 6d. During this time of operation, the emission spectra did not show any obvious changes in wavelength and intensity. These results indicated that the $CsPbBr_3$ PNCs-based SA was stable and promising for constructing Q-switched lasers in the telecommunication C-band window.

3. CONCLUSIONS

In summary, we have demonstrated $CsPbBr_3$ PNCs as a SA for generating Q-switched pulsed laser in telecommunication C-band. $CsPbBr_3$ PNCs with an average size of 20 nm were synthesized by a hot injection method. The excellent nonlinear saturable absorption property of $CsPbBr_3$ PNCs film at the C-band region was discovered and investigated. By inserting $CsPbBr_3$ SA into the EDFL cavity, stable Q-switched pulse laser operation was successfully achieved in the C-band region with a central wavelength of 1560 nm, a maximum pulsed repetition rate of 49.70 kHz, a maximum output power of 1.9 mW, and the shortest pulse duration of 5.96 μs. This work not only demonstrates that the $CsPbBr_3$ SA can be used as a promising candidate for pulsed laser generation in the telecommunication C-band region but also inspires further exploration of perovskite nanomaterials for potential applications in nonlinear optic, broadband ultrafast photonics, and optical communications.

AUTHOR INFORMATION

Corresponding Authors

Heng Jia − *College of Chemical Engineering, Inner Mongolia University of Technology, Hohhot, Inner Mongolia 010051, China*; orcid.org/0000-0003-0325-042X; Email: jiaheng17@mails.jlu.edu.cn

Nan Li − *Institute for Interdisciplinary Quantum Information Technology, Jilin Engineering Normal University, Changchun 130052, China*; Email: linan@jlenu.edu.cn

Authors

Shaohong Guo − *Inner Mongolia Key Laboratory of Green Catalysis and Inner Mongolia Collaborative Innovation Center for Water Environment Safety, College of Chemistry and Environmental Science, Inner Mongolia Normal University, Hohhot 010022, China*

Chunxia Li − *Inner Mongolia Key Laboratory of Green Catalysis and Inner Mongolia Collaborative Innovation Center for Water Environment Safety, College of Chemistry and Environmental Science, Inner Mongolia Normal University, Hohhot 010022, China*

Complete contact information is available at: https://pubs.acs.org/10.1021/acsomega.2c06107

Author Contributions

The manuscript was written through contributions of all authors. All authors have given approval to the final version of the manuscript.

Notes

The authors declare no competing financial interest.

ACKNOWLEDGMENTS

This work was supported by the Natural Science Foundation of Inner Mongolia of China (2021BS02019), the Research Foundation for Advanced Talents of Inner Mongolia Normal University (No. 2020YJRC012), the Research Project of the Inner Mongolia University of Technology (No. ZZ202108), the Scientific Research Startup Fund of Inner Mongolia University of Technology (DC2200000916), and the Natural Science Foundation of Jilin Province (YDZJ202201ZYTS324).

REFERENCES

(1) Fermann, M. E.; Hartl, I. Ultrafast Fibre Lasers. *Nat. Photonics* **2013**, *7*, 868−874.

(2) Shi, W.; Fang, Q.; Zhu, X.; Norwood, R. A.; Peyghambarian, N. Fiber Lasers and Their Applications. *Appl. Opt.* **2014**, *53*, 6554.

(3) Malinowski, A.; Gorman, P.; Codemard, C. A.; Ghiringhelli, F.; Boyland, A. J.; Marshall, A.; Zervas, M. N.; Durkin, M. K. High-Peak-Power, High-Energy, High-Average-Power Pulsed Fiber Laser System with Versatile Pulse Duration and Shape. *Opt. Lett.* **2013**, *38*, 4686.

(4) Kang, S.; Qiao, T.; Huang, X.; Yang, C.; Liu, X.; Qiu, J.; Yang, Z.; Dong, G. Enhanced CW Lasing and Q-Switched Pulse Generation Enabled by Tm^{3+}-Doped Glass Ceramic Fibers. *Adv. Opt. Mater.* **2021**, *9*, No. 2001774.

(5) Liu, X.; Guo, Q.; Qiu, J. Emerging Low-Dimensional Materials for Nonlinear Optics and Ultrafast Photonics. *Adv. Mater.* **2017**, *29*, No. 1605886.

(6) Xu, X. T.; Zhai, J. P.; Wang, J. S.; Chen, Y. P.; Yu, Y. Q.; Zhang, M.; Li, I. L.; Ruan, S. C.; Tang, Z. K. Passively Q-Switching Induced by the Smallest Single-Walled Carbon Nanotubes. *Appl. Phys. Lett.* **2014**, *104*, No. 171107.

(7) Zhang, B.; Liu, J.; Wang, C.; Yang, K.; Lee, C.; Zhang, H.; He, J. Recent Progress in 2D Material-Based Saturable Absorbers for All Solid-State Pulsed Bulk Lasers. *Laser Photonics Rev.* **2020**, *14*, No. 1900240.

(8) Fu, B.; Hua, Y.; Xiao, X.; Zhu, H.; Sun, Z.; Yang, C. Broadband Graphene Saturable Absorber for Pulsed Fiber Lasers at 1, 1.5, and 2 μm. *IEEE J. Sel. Top. Quantum Electron.* **2014**, *20*, 411−415.

(9) Martinez, A.; Sun, Z. Nanotube and Graphene Saturable Absorbers for Fibre Lasers. *Nat. Photonics* **2013**, *7*, 842−845.

(10) Yamashita, S.; Inoue, Y.; Maruyama, S.; Murakami, Y.; Yaguchi, H.; Jablonski, M.; Set, S. Y. Saturable Absorbers Incorporating Carbon Nanotubes Directly Synthesized onto Substrates and Fibers and Their Application to Mode-Locked Fiber Lasers. *Opt. Lett.* **2004**, *29*, 1581.

(11) Zhao, C.; Zhang, H.; Qi, X.; Chen, Y.; Wang, Z.; Wen, S.; Tang, D. Ultra-Short Pulse Generation by a Topological Insulator Based Saturable Absorber. *Appl. Phys. Lett.* **2012**, *101*, No. 211106.
(12) Yan, P.; Lin, R.; Ruan, S.; Liu, A.; Chen, H.; Zheng, Y.; Chen, S.; Guo, C.; Hu, J. A Practical Topological Insulator Saturable Absorber for Mode-Locked Fiber Laser. *Sci. Rep.* **2015**, *5*, No. 8690.
(13) Wen, X.; Gong, Z.; Li, D. Nonlinear Optics of Two-dimensional Transition Metal Dichalcogenides. *InfoMat* **2019**, *1*, 317−337.
(14) Wu, K.; Chen, B.; Zhang, X.; Zhang, S.; Guo, C.; Li, C.; Xiao, P.; Wang, J.; Zhou, L.; Zou, W.; Chen, J. High-Performance Mode-Locked and Q-Switched Fiber Lasers Based on Novel 2D Materials of Topological Insulators, Transition Metal Dichalcogenides and Black Phosphorus: Review and Perspective. *Opt. Commun.* **2018**, *406*, 214−229.
(15) Jia, H.; Li, N.; Li, S.; Liu, J.; Dong, Y.; Jia, Z.; Di, W.; Qin, G.; Qin, W. MnO_2 Nanosheets as Saturable Absorbers for a Q-Switched Fiber Laser. *Opt. Mater. Express* **2020**, *10*, 3097.
(16) Li, N.; Jia, H.; Guo, M.; Zhang, J.; Zhang, W. Y.; Guo, Z. X.; Li, M. X.; Jia, Z. X.; Qin, G. S. Broadband Fe_3O_4 Nanoparticles Saturable Absorber for Q-Switched Fiber Lasers. *Opt. Fiber Technol.* **2021**, *61*, No. 102421.
(17) Wang, F.; Chen, H.; Lan, D.; Zhang, F.; Sun, Y.; Zhang, X.; Li, S.; Cheng, T. Highly Efficient and Robust Broadband Nano-VO_2 (M) Saturable Absorber for Nonlinear Optics and Ultrafast Photonics. *Adv. Opt. Mater.* **2021**, *9*, No. 2100795.
(18) Li, N.; Jia, H.; Guo, M.; Zhang, W.; Wang, J.; Song, L. Nano-Cs_xWO_3: Ultra-Broadband Nonlinear Optical Modulator for Near-Infrared and Mid-Infrared Ultrafast Fiber Lasers Generation. *Nano Res.* **2022**, *15*, 4403−4410.
(19) Fu, B.; Sun, J.; Cheng, Y.; Ouyang, H.; Compagnini, G.; Yin, P.; Wei, S.; Li, S.; Li, D.; Scardaci, V.; Zhang, H. Recent Progress on Metal-Based Nanomaterials: Fabrications, Optical Properties, and Applications in Ultrafast Photonics. *Adv. Funct. Mater.* **2021**, *31*, No. 2107363.
(20) Zhang, M.; Wu, Q.; Zhang, F.; Chen, L.; Jin, X.; Hu, Y.; Zheng, Z.; Zhang, H. 2D Black Phosphorus Saturable Absorbers for Ultrafast Photonics. *Adv. Opt. Mater.* **2019**, *7*, No. 1800224.
(21) Chen, H.; Wang, F.; Liu, M.; Qian, M.; Men, X.; Yao, C.; Xi, L.; Qin, W.; Qin, G.; Wu, C. Near-Infrared Broadband Polymer-Dot Modulator with High Optical Nonlinearity for Ultrafast Pulsed Lasers. *Laser Photonics Rev.* **2019**, *13*, No. 1800326.
(22) Chen, H.; Wang, F.; Qian, M.; Zhou, X.; Li, Z.; Cheng, T.; Qin, G. Semiconducting Polymer Dots as Broadband Saturable Absorbers for Q-Switched Fiber Lasers. *J. Mater. Chem. C* **2020**, *8*, 4919−4925.
(23) Wang, F.; Jing, Y.; Kang, Z.; Zhou, L.; Li, Z.; Liu, M.; Wang, T.; Yao, C.; Chen, H.; Qin, W.; Qiao, Z.-A.; Qin, G.; Wu, C. Mesoporous Carbon Nanospheres as Broadband Saturable Absorbers for Pulsed Laser Generation. *Adv. Opt. Mater.* **2018**, *6*, No. 1800606.
(24) Lee, J.; Koo, J.; Chi, C.; Lee, J. H. All-Fiberized, Passively Q-Switched 1.06 μm Laser Using a Bulk-Structured Bi_2Te_3 Topological Insulator. *J. Opt.* **2014**, *16*, No. 085203.
(25) Özbal, G.; Senger, R. T.; Sevik, C.; Sevinçli, H. Ballistic Thermoelectric Properties of Monolayer Semiconducting Transition Metal Dichalcogenides and Oxides. *Phys. Rev. B* **2019**, *100*, No. 085415.
(26) Alani, I. A. M.; Lokman, M. Q.; Ahmed, M. H. M.; Al-Masoodi, A. H. H.; Latiff, A. A.; Harun, S. W. A Few-Picosecond and High-Peak-Power Passively Mode-Locked Erbium-Doped Fibre Laser Based on Zinc Oxide Polyvinyl Alcohol Film Saturable Absorber. *Laser Phys.* **2018**, *28*, No. 075105.
(27) de Weerd, C.; Gregorkiewicz, T.; Gomez, L. All-Inorganic Perovskite Nanocrystals: Microscopy Insights in Structure and Optical Properties. *Adv. Opt. Mater.* **2018**, *6*, No. 1800289.
(28) Zhou, Y.; Chen, J.; Bakr, O. M.; Mohammed, O. F. Metal Halide Perovskites for X-Ray Imaging Scintillators and Detectors. *ACS Energy Lett.* **2021**, *6*, 739−768.
(29) Shen, W.; Chen, J.; Wu, J.; Li, X.; Zeng, H. Nonlinear Optics in Lead Halide Perovskites: Mechanisms and Applications. *ACS Photonics* **2021**, *8*, 113−124.
(30) Xu, J.; Li, X.; Xiong, J.; Yuan, C.; Semin, S.; Rasing, T.; Bu, X. Halide Perovskites for Nonlinear Optics. *Adv. Mater.* **2020**, *32*, No. 1806736.
(31) Wang, G.; Mei, S.; Liao, J.; Wang, W.; Tang, Y.; Zhang, Q.; Tang, Z.; Wu, B.; Xing, G. Advances of Nonlinear Photonics in Low-Dimensional Halide Perovskites. *Small* **2021**, *17*, No. 2100809.
(32) Mushtaq, A.; Pradhan, B.; Kushavah, D.; Zhang, Y.; Wolf, M.; Schrenker, N.; Fron, E.; Bals, S.; Hofkens, J.; Debroye, E.; Pal, S. K. Third-Order Nonlinear Optical Properties and Saturation of Two-Photon Absorption in Lead-Free Double Perovskite Nanocrystals under Femtosecond Excitation. *ACS Photonics* **2021**, *8*, 3365−3374.
(33) Zhou, Y.; Hu, Z.; Li, Y.; Xu, J.; Tang, X.; Tang, Y. $CsPbBr_3$ Nanocrystal Saturable Absorber for Mode-Locking Ytterbium Fiber Laser. *Appl. Phys. Lett.* **2016**, *108*, No. 261108.
(34) Li, J.; Dong, H.; Xu, B.; Zhang, S.; Cai, Z.; Wang, J.; Zhang, L. $CsPbBr_3$ Perovskite Quantum Dots: Saturable Absorption Properties and Passively Q-Switched Visible Lasers. *Photonics Res.* **2017**, *5*, 457.
(35) Liu, B.; Gao, L.; Cheng, W. W.; Tang, X. S.; Gao, C.; Cao, Y. L.; Li, Y. J.; Zhu, T. 1.6 μm Dissipative Soliton Fiber Laser Mode-Locked by Cesium Lead Halide Perovskite Quantum Dots. *Opt. Express* **2018**, *26*, 7155.
(36) Zhou, Y.; Zhang, R.; Li, X.; Kuan, P.; He, D.; Hou, J.; Liu, Y.; Fang, Y.; Liao, M. $CsPbBr_3$ Nanocrystal for Mode-Locking Tm-Doped Fiber Laser. *Chin. Phys. B* **2019**, *28*, No. 094203.
(37) Guo, P.; Li, X.; Chai, T.; Feng, T.; Ge, Y.; Song, Y.; Wang, Y. Few-Layer Bismuthene for Robust Ultrafast Photonics in C-Band Optical Communications. *Nanotechnology* **2019**, *30*, No. 354002.
(38) Fu, Y.; Yang, Y.; Sun, T.; Tang, Y.; Li, J.; Cui, H.; Qin, W.; Wang, F.; Qin, G.; Zhao, D. Polymer-Based S-Band Waveguide Amplifier Using $NaYF_4$:Yb,Tm−PMMA Nanocomposite as Gain Medium. *Opt. Lett.* **2022**, *47*, 154.
(39) Guo, S. H.; Zhou, J.; Zhao, X.; Sun, C. Y.; You, S. Q.; Wang, X. L.; Su, Z. M. Enhanced CO_2 Photoreduction via Tuning Halides in Perovskites. *J. Catal.* **2019**, *369*, 201−208.
(40) Gao, G.; Xi, Q.; Zhou, H.; Zhao, Y.; Wu, C.; Wang, L.; Guo, P.; Xu, J. Novel Inorganic Perovskite Quantum Dots for Photocatalysis. *Nanoscale* **2017**, *9*, 12032−12038.
(41) Wang, J.; Hernandez, Y.; Lotya, M.; Coleman, J. N.; Blau, W. J. Broadband Nonlinear Optical Response of Graphene Dispersions. *Adv. Mater.* **2009**, *21*, 2430−2435.
(42) Li, P.; Chen, Y.; Yang, T.; Wang, Z.; Lin, H.; Xu, Y.; Li, L.; Mu, H.; Shivananju, B. N.; Zhang, Y.; Zhang, Q.; Pan, A.; Li, S.; Tang, D.; Jia, B.; Zhang, H.; Bao, Q. Two-Dimensional $CH_3NH_3PbI_3$ Perovskite Nanosheets for Ultrafast Pulsed Fiber Lasers. *ACS Appl. Mater. Interfaces* **2017**, *9*, 12759−12765.

https://doi.org/10.1021/acsomega.2c06107
ACS Omega 2022, 7, 45504−45509